

# Supervised and Unsupervised Tumor Characterization in the Deep Learning Era

Sarfaraz Hussein, Maria M. Chuquicusma, Pujan Kandel, Candice W. Bolan, Michael B. Wallace, and Ulas Bagci\*, *Senior Member, IEEE*.

**Abstract**—Computer Aided Diagnosis (CAD) tools are often needed for fast and accurate detection, characterization, and risk assessment of different tumors from radiology images. Any improvement in robust and accurate image-based *tumor characterization* can assist in determining non-invasive cancer stage, prognosis, and personalized treatment planning as a part of precision medicine. In this study, we propose both supervised and unsupervised machine learning strategies to improve tumor characterization. Our *first approach* is based on supervised learning for which we demonstrate significant gains in deep learning algorithms, particularly Convolutional Neural Network (CNN), by utilizing completely 3D approach and *transfer learning* to address the requirements of volumetric and large amount of training data, respectively. Motivated by the radiologists’ interpretations of the scans, we then show how to incorporate task dependent feature representations into a CAD system via a graph regularized sparse Multi-Task Learning (MTL) framework.

In the *second approach*, we explore an unsupervised scheme in order to address the limited availability of labeled training data, a common problem in medical imaging applications. Inspired by learning from label proportion (LLP) approaches, we propose a new algorithm, *proportion-SVM*, to characterize tumor types. In this second approach, we also seek the answer to the fundamental question about the goodness of “deep features” for unsupervised tumor classification. Finally, we study the effect of unsupervised representation learning using *Generative Adversarial Networks (GAN)* on classification performance. We evaluate our proposed approaches (both supervised and unsupervised) on two different tumor diagnosis challenges: lung and pancreas with 1018 CT and 171 MRI scans respectively.

**Index Terms**—Computer-Aided Diagnosis (CAD), Lung cancer, Pancreatic Cancer, 3D Convolutional Neural Network, Magnetic Resonance Imaging (MRI), Computed Tomography (CT), Deep learning

## I. INTRODUCTION

Cancer affects a significant number of the world’s population; approximately 39.6% of men and women will be diagnosed with cancer at some point during their lifetime with an overall mortality of 171.2 per 100,000 men and women per year (based on 2008-2012 deaths) [1]. Lung and pancreatic cancers are two of the most common cancers. While lung cancer is the largest cause of cancer-related deaths in the world, pancreatic cancer has the poorest prognosis with a 5-year survival rate of just 7% in the United States [1]. Out of 8.2 million deaths due to cancer worldwide, lung cancer accounts for the highest number of mortalities i.e. 1.59 million [1].

\* indicates corresponding author (ulasbagci@gmail.com).

S. Hussein, M. Chuquicusma, and U. Bagci are with Center for Research in Computer Vision (CRCV) at University of Central Florida (UCF), Orlando, FL; P. Kandel, C. Bolan and M. Wallace are with Mayo Clinic, Jacksonville, FL

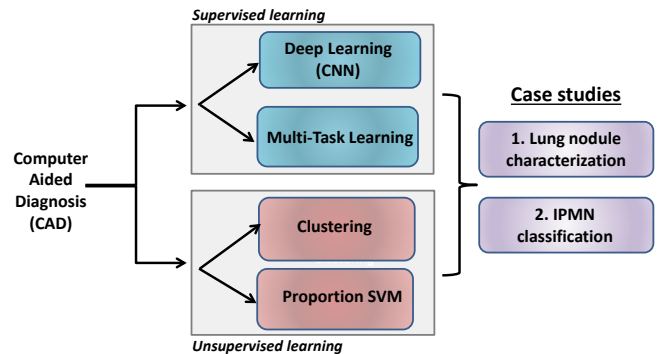


**Figure 1:** A block diagram to represent different schemes, methods and experimental case studies presented in this paper. We categorize CAD systems into supervised and unsupervised schemes. For supervised scheme, we propose a new algorithm consisting of a 3D CNN architecture and Graph Regularized Sparse Multi-task learning and perform evaluations for lung nodule characterization. For unsupervised scheme, we proposed a new clustering algorithm,  $\alpha$ -SVM, and test it for the classification of lung nodules and IPMN.

With regards to pancreatic cancer, specifically in this work, we focus on the challenging problem of automatic diagnosis of Intraductal Papillary Mucinous Neoplasms (IPMN), which is a pre-malignant condition and if left untreated, it can progress to invasive cancer. IPMN is mucin-producing neoplasm that can be found in the main pancreatic duct and its branches. They are radiographically identifiable precursors to pancreatic cancer [2]. Detection and characterization of these lung and pancreatic tumors can aid in early diagnosis and in identifying cancer stages for improved treatment and increased chances of survival. In addition, any significant improvement in developing supervised and unsupervised techniques geared toward accurate Computer Aided Diagnosis (CAD) systems can save significant manual exertion, as well as valuable time.

Conventionally, the CAD systems are designed to assist radiologists in making accurate and fast clinical decisions by reducing the number of false positives and false negatives. For diagnostic decision making, a higher emphasis is laid on increased sensitivity as a false-flag is more tolerable than a tumor being missed or incorrectly classified as benign. In this regard, research in developing CAD algorithms can help explore the domain of imaging features and markers which can be then studied by radiologists to further improve clinical decisions. In the literature, automated detection and diagnosis

methods had been developed for tumors in different organs such as breast, colon, brain, lung, liver, prostate, and others. Generally, a CAD system comprises preprocessing, feature engineering, which includes feature extraction and selection followed by a classification scheme. However, with the success of deep learning, the medical imaging community has moved from feature engineering to feature learning. In those frameworks, Convolutional Neural Networks (CNN) had been used for feature extraction and an off-the-shelf classifier, such as Random Forest (RF) was employed for classification [3], [4].

This work is an extension to our IPMI 2017 [5] work. We first propose a supervised strategy to address the challenge of risk-stratification of lung nodules in low-dose CT scans. Capitalizing on the significant progress of deep learning technologies for image classification and their potential applications in radiology [6], we propose a 3D CNN based approach for rich feature representation of lung nodules. We argue that the use of 3D CNN is paramount in the classification of lung nodules in low-dose CT scans which are 3D by nature. By using the conventional 2D CNN methods, however, we implicitly lose the important volumetric information which can be very significant for accurate risk stratification. The superior performance of 3D CNN over 2D networks is well studied in [7]. We also avoid hand-crafted feature extraction, painstaking feature engineering, and parameter tuning. Inspired by the significance of lung nodule attributes for clinical determination of malignancy [8], we utilize the information about six high-level nodule attributes such as calcification, sphericity, margin, lobulation, spiculation, and texture (Figure 2-A) to improve automatic benign-malignant classification. Furthermore, we identify features corresponding to these high-level nodule attributes and fuse them in a multi-task learning (MTL) framework to obtain the final risk assessment scores.

We also explore the potential of unsupervised learning for lung nodule and IPMN classification. Inspired by the successful application of unsupervised methods in other domains, we study to extract important discriminative information from a large amount of unlabeled data. We employ both hand-crafted and deep learning features extracted from pre-trained networks for classification. In order to obtain an initial set of labels in an unsupervised fashion, we cluster the samples into different groups in the feature domain. We next propose to train *Proportion-Support Vector Machine* ( $\propto$ SVM) classifier using label proportions rather than instance labels. The trained model is then employed to classify testing samples as benign or malignant.

## II. RELATED WORK

In this section, we summarize the advances in machine learning applied to medical imaging and CAD systems developed for lung cancer diagnosis. Since the automatic characterization of IPMN has not been extensively studied in the literature, relevant works are selected from the clinical studies. Our work will be the first in this regard.

**Imaging Features and Classifiers:** Conventionally, the characterization of lung nodules involves nodule segmentation,

extraction of hand-crafted imaging features, followed by the application of an off-the-shelf classifier/regressor. The method by [9], for instance, was based on the extraction of various physical measures, including intensity statistics and then classification using Artificial Neural Networks. El-Baz et al. [10] first segmented the lung nodules using appearance-based models and used spherical harmonic analysis to perform shape analysis. The final step was the classification using  $k$ -nearest neighbor. Proposing a study based on texture analysis, [11] extracted 2D texture features such as Haralick, Gabor and Local Binary Patterns (LBP) and extended them to 3D. A Support Vector Machine (SVM) was employed to perform the classification. In another classical work by [12], segmentation is performed using 3D active contours followed by the extraction of texture features from the rubber band straightening transform of the surrounding voxels. The classification was performed using Linear Discriminant Analysis (LDA) classifier. In another study, [13] proposed a feature selection based approach using both imaging and clinical data. An ensemble classifier, combining genetic algorithm (GA) and random subspace method (RSM) was then used to gauge feature relevance and information content. At the final step, LDA was employed to perform classification on the reduced feature set. More recently, [4] combined spherical harmonics along with deep CNN features and then classified them using RF. Yet, the use of CNN for lung nodule classification has been confined to 2D image analysis [14], thus falling short of utilizing the important volumetric and contextual information.

**Image Attributes:** The use of high-level image attributes had been found to be instrumental in the risk assessment and classification of lung nodules. In an effort to study the relationship between nodule attributes and malignancy, [8] found that 82% of the lobulated, 97% of the densely spiculated, 93% of the ragged and 100% of the halo nodules were malignant in a particular dataset. Moreover, 66% of the round nodules were found to be benign. Inspired by this study, in this work we utilize 3D CNN to learn discriminative feature set corresponding to each of the 6 attributes. We then fuse these feature representations via MTL to determine the malignancy likelihood.

**IPMN:** Although there has been a considerable progress in developing automatic approaches to segment pancreas and its cysts [15], [16], the use of CAD systems to perform fully automatic risk-stratification of IPMNs is limited. For instance, the approach by [17] investigated the influence of 360 imaging features ranging from intensity, texture, and shape to stratify subjects as low or high-grade IPMN. In another example, [18] extracted texture and features from solid component of segmented cysts followed by a feature selection and classification scheme. Here it is important to note that both of these approaches [18], [17] required segmentation of cysts or pancreas and are evaluated on CT scans. In contrast, our experimental setup doesn't require segmentation of cysts or pancreas and we evaluate IPMNs on MRI scan which is a preferred imaging modality because of

no radiation exposure and improved soft-tissue contrast [19]. To the best of our knowledge, our study is the largest IPMN classification study consisting of 171 subjects across both modalities (CT and MRI).

**Unsupervised Learning:** Typically, the visual recognition and classification tasks are addressed using supervised learning algorithms which use labeled data. However, for tasks where manually generating labels corresponding to large datasets is laborious and expensive, the use of unsupervised learning methods is of significant value. Unsupervised techniques had been used to solve problems in various domains ranging from object categorization [20] to speech processing [21]. These methods typically relied on some complementary information provided with the data to improve learning, which may not be available for many classification tasks in medical imaging.

### Our Contributions

A block diagram representing different supervised and unsupervised schemes is presented in Figure 1. Overall, our main contributions in this work can be summarized as follows:

- For supervised learning, we propose a 3D CNN based method to utilize the volumetric information from a CT scan, which would be otherwise lost in the conventional 2D CNN based approaches. We also circumvent the need for a large amount of volumetric training data to train the 3D network by transfer learning. We use the CT data to fine-tune a network which is trained on 1 million videos. To the best of our knowledge, our work is the first to empirically validate the success of transfer learning of a 3D network for lung nodules. Furthermore, we employ graph regularized sparse MTL to fuse the complementary feature information from high-level nodule attributes for malignancy determination. Figure 2-A shows lung nodule attributes with different levels of prominence.

As an extension of our IPMI 2017 work [5], we made the following additional contributions in this paper:

- We propose and evaluate different supervised and unsupervised methods for both lung nodules and IPMN diagnosis. In the era where the wave of deep learning has swept into almost all domains of visual analysis, we investigate the contribution of features extracted from different deep learning architectures. Moreover, we also study the effect of unsupervised representation learning using Generative Adversarial Networks (GANs) on classification performance.
- Our work can be considered as a significant milestone to study the potential of unsupervised learning methods for the lung nodule and IPMN classification using both handcrafted and deep learning features. Additionally, in order to alleviate the effect of noisy labels (i.e. mislabeling) obtained during clustering, we propose to employ  $\alpha$ SVM, which is trained on label proportions. Instead of hard assigning labels, we estimate the label proportions in a data-driven manner. We experimentally establish that learning a discriminative

model using the proposed combination of clustering and  $\alpha$ SVM is superior in performance as compared to training a classifier with noisy instance level labels.

Other than these contributions, we have also extended the evaluation set to include IPMN diagnosis with MRI scans on a dataset consisting of over 170 scans. To our best of knowledge, no previous study has investigated automatic diagnosis of IPMN with MRI.

## III. SUPERVISED LEARNING METHODS

### A. Problem Formulation

Let  $X = [x_1, x_2 \dots x_n] \in \mathbb{R}^{n \times d}$  be the data matrix comprising features from  $n$  data samples with dimension  $d$  ( $\in \mathbb{R}^d$ ). Each data sample corresponds to a regression score given by  $Y = [y_1, y_2 \dots y_n]$ , where  $Y \in \mathbb{R}^{n \times 1}$ . Generally, in CAD systems,  $X$  consists of features extracted from images, and  $Y$  represents probability values indicating the likelihood of being malignant or benign. The objective in supervised learning is to learn the coefficient vector or the regression estimator  $W$  from the training data, where the ground truth labels are known. While testing,  $W$  will then be used to estimate  $Y$  for an unseen testing example. For regression, a regularizer is added to prevent over-fitting. In this case, the  $\ell_1$  regularized least square regressor is commonly defined as:

$$\min_W \|XW - Y\|_2^2 + \lambda \|W\|_1, \quad (1)$$

where  $\lambda$  controls the sparsity level of the coefficient vector  $W = [w_1, w_2 \dots w_d]$ . The problem in Eq. 1 is an *unconstrained convex optimization* problem, and it remains non-differentiable when  $w_i = 0$ . The closed form solution corresponding to the global minimum for Eq. 1 is not possible. Thus, the above equation is turned into a *constrained optimization* function in the following way:

$$\min_W \|XW - Y\|_2^2, \text{ s.t. } \|W\|_1 \leq t, \quad (2)$$

where  $t$  is inversely proportional to  $\lambda$ . In the representation given in Eq. 2, both optimization function and the constraint are convex, hence global minimum is now a possibility. In the following subsections, we extend this supervised setting in deep learning and MTL to characterize nodules as benign or malignant.

### B. Transfer Learning for Lung Nodule Characterization

We use the lung nodules dataset to fine-tune a 3D CNN [7] trained on Sports-1M dataset [23]. The sports dataset includes 1 million videos with 487 classes. In the absence of a large number of training examples from lung nodules, we use transfer learning strategy to obtain rich feature representation from a larger dataset (Sports-1M) for lung nodule characterization. The 3D network comprises 5 convolution, 5 max-pooling, 2 fully-connected and 1 soft-max classification layers. The input to the network is  $3 \times 16 \times 128 \times 171$ , where there are 16 non-overlapping slices in the input volume. The first 2 convolution

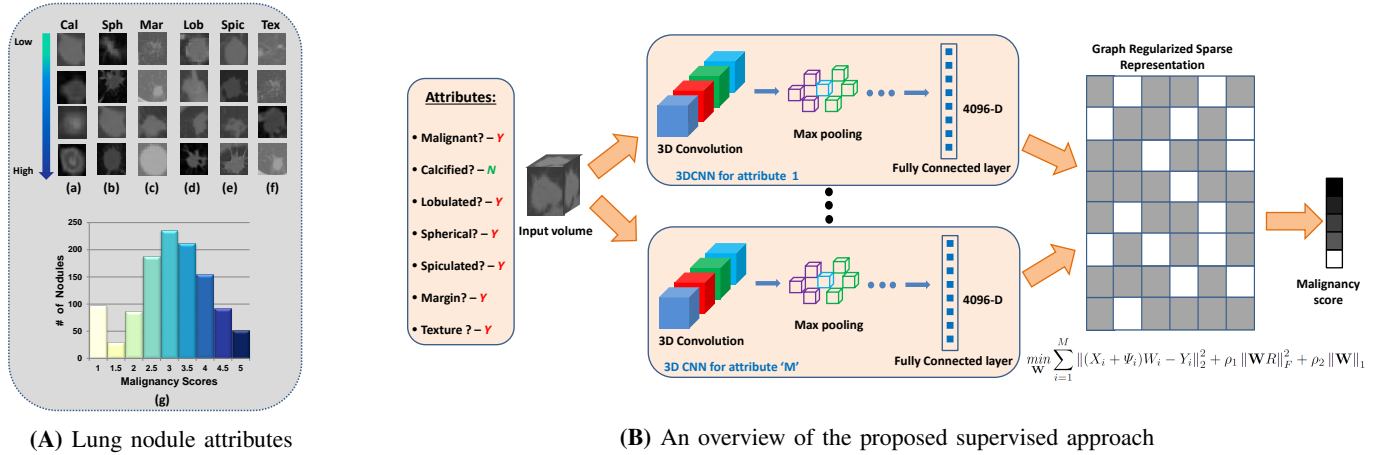


**Figure 2:** (A) Lung nodule attributes with different scores. As we move from the top (attribute missing) to the bottom (attribute with the highest prominence), the prominence of the attributes increases. (a-f) show different attributes including calcification, sphericity, margin, lobulation, spiculation and texture. The graph in (g) shows the number of nodules with different malignancy scores in our experiments using the publicly available dataset [22]. (B) shows an overview of the proposed 3D CNN based graph regularized sparse MTL approach.

layers have 64 and 128 filters respectively, whereas there are 256 filters in the last 3 layers. The outputs of the fully connected layers are of 4096 dimensions.

### C. Multi-task learning (MTL)

We formulate the malignancy determination of lung nodules as an MTL problem, where different tasks represent different attributes of a nodule. Here the aim is to learn a joint model while exploiting the dependencies among attributes (tasks) in feature space. Consider a problem with  $M$  tasks representing different attributes corresponding to a given dataset  $D$ . These tasks may be related and share some feature representation, both of which are unknown. The goal in MTL is to perform joint learning of these tasks while exploiting dependencies in the feature space so as to improve regressing one task using the others. In contrast to multi-label learning, tasks may have different features in MTL.

As shown in Figure 2-B, we design lung tumor characterization as an MTL problem, where each task has model parameters denoted by  $W_m$ , used to regress the corresponding task  $m$ . Moreover, when  $\mathbf{W} = [W_1, W_2 \dots W_M] \in \mathbb{R}^{M \times d}$  represents a rectangular matrix, rank is considered as an extension to the cardinality. In that case, trace norm, which is the sum of singular values is a replacement to the  $\ell_1$ -norm. Trace norm, also known as nuclear norm is the convex envelope of the rank of a matrix (which is non-convex), where the matrices are considered on a unit ball. By replacing  $\ell_1$ -norm with trace norm in Eq. 1, the trace norm regularized least square loss function is given by:

$$\min_{\mathbf{W}} \sum_{i=1}^M \|X_i W_i - Y_i\|_2^2 + \rho \|\mathbf{W}\|_*, \quad (3)$$

where  $\rho$  tunes the rank of the matrix  $\mathbf{W}$ , and trace-norm is defined as:  $\|\mathbf{W}\|_* = \sum_{i=1} \sigma_i(\mathbf{W})$  with  $\sigma$  representing singular values.

As the task relationships are often unknown and are learned from data, we represent tasks and their relations in the form of a graph. Consider a complete graph  $\Upsilon = (V, E)$ , such that nodes  $V$  represent the tasks and the edges  $E$  encode any relativity between the tasks. A regularizer, pertinent to MTL, is the regularization on the graph representing the relationship between the tasks [24]. The complete graph can be represented as a structure matrix  $S = [e^1, e^2 \dots e^{|E|}]$  and the difference between all the pairs connected in the graph is penalized by the following regularizer:

$$\|\mathbf{W}S\|_F^2 = \sum_{i=1}^{|E|} \|\mathbf{W}e^i\|_2^2 = \sum_{i=1}^{|E|} \|\mathbf{W}_{e_a^i} - \mathbf{W}_{e_b^i}\|_2^2, \quad (4)$$

here,  $e_a^i, e_b^i$  are the edges between the nodes  $a$  and  $b$ . The above regularizer can also be written as:

$$\|\mathbf{W}S\|_F^2 = \text{tr}((\mathbf{W}S)^T(\mathbf{W}S)) = \text{tr}(\mathbf{W}S S^T \mathbf{W}^T) = \text{tr}(\mathbf{W} \mathcal{L} \mathbf{W}^T), \quad (5)$$

where ‘tr’ represents the trace of a matrix and  $\mathcal{L} = S S^T$  is the Laplacian matrix.

There may exist disagreements between the scores from different experts (radiologists) due to the inherent uncertainty in their evaluations. For instance, while one radiologist may give a malignancy score of  $x_1^j$  to a nodule  $j$ , the other may give a score of  $x_2^j$ . In order to reflect these uncertainties in our algorithm, we propose a scoring function to measure such inconsistencies:

$$\Psi(j) = \left( \exp\left(-\frac{\sum_i (x_i^j - \mu^j)^2}{2\sigma^p}\right) \right)^{-1}. \quad (6)$$

This inconsistency measure, corresponding to a particular example  $j$ , is represented by  $\Psi(j)$ .  $x_i^j$  is the score given by the expert (radiologist)  $i$  and  $\mu^j$  and  $\sigma^j$  denote mean and

standard deviation of the scores, respectively. For simplicity, we have dropped the index for the task; however, note that the inconsistency measure is computed for all the tasks. The final proposed graph regularized sparse least square optimization function with the inconsistency measure can then be written as:

$$\min_{\mathbf{W}} \sum_{i=1}^M \underbrace{\|(X_i + \Psi_i)W_i - Y_i\|_2^2}_{\textcircled{1}} + \underbrace{\rho_1 \|\mathbf{W}S\|_F^2}_{\textcircled{2}} + \underbrace{\rho_2 \|\mathbf{W}\|_1}_{\textcircled{3}}, \quad (7)$$

where  $\rho_1$  controls the level of penalty for graph structure and  $\rho_2$  controls the sparsity. In the above optimization, the least square loss function ① considers tasks to be decoupled whereas ② and ③ consider the interdependencies between different tasks.

#### D. Optimization

The optimization function in Eq. 7 cannot be solved through standard gradient descent because the  $\ell_1$ -norm is not differentiable at  $\mathbf{W} = 0$ . Since the optimization function in Eq. 7 has both smooth and non-smooth convex parts, estimating the non-smooth part can help solve the optimization function. Therefore, *accelerated proximal gradient method* [25] is employed to solve the Eq. 7. The accelerated proximal method is the first order gradient method with a complexity of  $O(1/k^2)$ , where  $k$  is the iteration counter. Note that in Eq. 7, the  $\ell_1$ -norm comprises the non-smooth part and the proximal operator is used for its estimation.

### IV. UNSUPERVISED LEARNING METHODS

Since in medical imaging, the task of generating image labels is laborious, expensive, and time-consuming, we explore the potential of unsupervised learning approaches for developing CAD systems. Our proposed unsupervised framework includes three steps (Figure 3). First, we perform clustering on the appearance features obtained from the images to estimate an initial set of labels. Using the obtained initial labels, we compute label proportions corresponding to each cluster. We finally train a classifier using the label proportions and clusters to obtain the final classification.

#### A. Initial Label Estimation

Let  $X = [x_1, x_2 \dots x_n] \in \mathbb{R}^{n \times d}$  represents the input matrix which contains features from  $n$  images such that  $x \in \mathbb{R}^d$ . In order to obtain an initial set of labels corresponding to each sample, we cluster the data into  $2 \leq k < n$  clusters using  $k$ -means. Let  $M$  represents  $|X| \times k$  membership matrix which denotes the membership assignment of each sample to a cluster. The optimal clustering would minimize the following objective function:

$$\operatorname{argmin}_M \sum_{j=1}^k M(i, j) \|x_i - \mu_j\|^2, \quad (8)$$

where  $\mu_j$  is the mean of the samples in cluster  $j$ . The label  $y_i$  for the  $i^{\text{th}}$  sample can then be estimated as:

$$y_i = \operatorname{argmax}_j M(i, j) \quad (9)$$

These labels serve as an initial set used to estimate label proportions which are then used to train proportion-SVM ( $\propto$ SVM) for further improvements.

#### B. Learning with the Estimated Labels

Since our initial label estimation approach is unsupervised, there are uncertainties associated with them. It is, therefore, reasonable to assume that learning a discriminative model based on these noisy instance level labels can deteriorate classification performance. In order to address this issue, we model the instance level labels as *latent* unknown variables and thereby consider group/bag level labels.

Inspired by  $\propto$ SVM approach [26], which models the latent instance level variables using the known group level label proportions, we formulate our learning problem such that clusters are analogous to the groups. In our formulation, each cluster  $j$  can be represented as a group such that the majority of samples belong to the class  $j$ . Considering the groups to be disjoint such that  $\bigcup_{j=1}^k \Omega_j = 1, 2, \dots, n$ , and  $\Omega$  represents groups; the objective function of the large-margin  $\propto$ SVM after convex relaxation can be formulated as:

$$\min_{\mathbf{y} \in \mathcal{Y}} \min_w \left( \frac{1}{2} w^T w + C \sum_{i=1}^n L(y_i, w^T \phi(x)) \right) \quad (10)$$

$$\mathcal{Y} = \left\{ \mathbf{y} \mid |\tilde{p}_j - p_j| \leq \epsilon, y_i \in \{-1, 1\} \forall j \right\},$$

where  $\tilde{p}$  and  $p$  represent the estimated and true label proportions, respectively. In Eq. 10,  $\mathbf{y}$  is the set of instance level labels,  $\phi(\cdot)$  is the input feature,  $C$  denotes cost parameter and  $L(\cdot)$  represents the hinge-loss function for maximum-margin classifiers such as SVM.

The optimization in Eq.10 is, in fact, an instance of Multiple Kernel Learning, which can be solved using the cutting plane method where the set of active constraints is incrementally computed. The goal is to find the most violated constraint, which is further relaxed by aiming for any violated constraint.

#### C. Calculating Label Proportions

In the conventional  $\propto$ SVM approach, the label proportions are known a priori. Since our approach is unsupervised, both instance level labels and group label proportions are unknown. Moreover, establishing strong assumptions about the label proportions may affect learning. It is, however, reasonable to assume that a large number of instances in any group carry the same label and there may be a small number of instances which are outliers. In order to determine the label proportions in a data-driven manner, we use the estimated labels obtained from clustering. The label proportion  $p_j$  corresponding to the group  $j$  can be represented as:

$$p_j = n^{-1} \sum_{i=1}^n I(y_i = j), \quad (11)$$

where  $I(\cdot)$  is the indicator function which returns 1 when  $y_i = j$ . The  $\propto$ SVM is trained using the image features and label proportions to classify the testing data. It is important to mention that since our approach is unsupervised we don't use

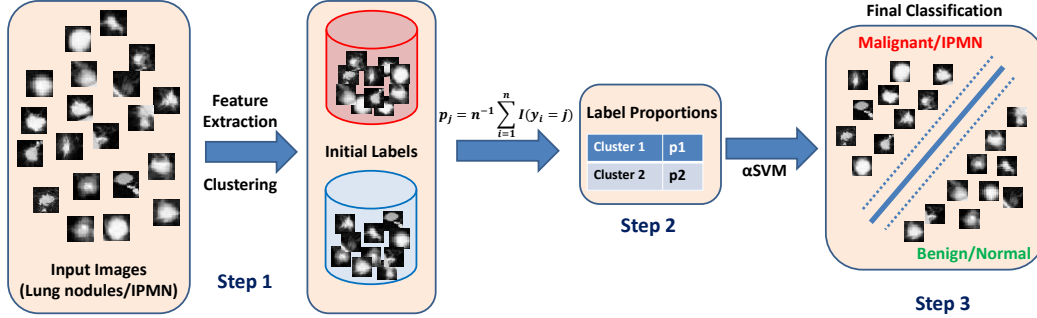


**Figure 3:** An overview of the proposed unsupervised approach. Given the input images, we compute GIST features and perform  $k$ -means clustering to obtain the initial set of labels which can be noisy. Using the set of labels, we compute label proportions corresponding to each cluster/group (Eq. 11). We finally employ  $\alpha$ SVM to learn a discriminative model using the features and label proportions.

the ground truth labels for training rather they are only used for evaluations. In addition, clustering and label proportion calculation are only performed on the training data and the testing data remains completely unseen for  $\alpha$ SVM.

## V. EXPERIMENTS

### A. Data for Lung Nodules

For evaluating our proposed approach, we used LIDC-IDRI dataset from Lung Image Database Consortium [22], which is one of the largest publicly available lung cancer screening datasets. There were 1018 CT scans in the dataset, where the slice thickness varied from 0.45 mm to 5.0 mm. The nodules having diameters larger than or equal to 3 mm were annotated by at most four radiologists.

The nodules which were annotated by at least three radiologists were used for the evaluations. There were 1340 nodules satisfying this criterion. We used the mean malignancy and attribute scores of different radiologists for experiments. The nodules have ratings corresponding to malignancy and the other six attributes which are (i) calcification, (ii) lobulation, (iii) spiculation, (iv) sphericity, (v) margin and (vi) texture (Figure 2). The malignancy ratings varied from 1 to 5 where 1 indicated benign and 5 represented highly malignant nodules. We excluded nodules with an average score equal to 3 to account for the indecision among the radiologists. Our final dataset consisted of 635 benign and 509 malignant nodules for classification. The images were resampled to have 0.5 mm spacing in each dimension.

### B. Data for IPMN

The data for the classification of IPMN contains T2 MRI axial scans from 171 subjects. The scans were labeled by a radiologist as normal or IPMN. Out of 171 scans, 38 subjects were normal, whereas the rest of 133 were from subjects diagnosed with IPMN. The in-plane spacing (xy-plane) of the scan was ranging from 0.468 mm to 1.406 mm. As pre-processing, we first employ N4 bias field correction [27] to each image in order to normalize variations in image intensity. We then apply curvature anisotropic image filter to smooth

**TABLE I:** Classification accuracy and mean absolute score difference of the proposed multi-task learning method in comparison with the other methods of lung nodules characterization

Methods	Accuracy	Mean score diff.
GIST features with LASSO	76.83%	0.675
3D CNN MTL with Trace norm	80.08%	0.625
<b>Proposed (MTL, Eq. 7)</b>	<b>91.26%</b>	<b>0.459</b>

image while preserving edges. For experiments, 2D axial slices with pancreas (and IPMN) are cropped to generate Region of Interest (ROI) as shown in Figure 4. The large intra-class variation, especially due to varying shapes of the pancreas can also be observed in Figure 4.

### C. Evaluation and Results- Supervised Learning

We evaluated the graph regularized sparse MTL on lung nodules dataset since it contained attribute scores from radiologists. We used the 3D CNN trained on Sports-1M dataset [23] which had 487 classes. We fine-tuned the network using samples from lung nodule dataset. In order to generate the binary labels for the six attributes and the malignancy, we used the center point and gave positive (or negative) labels to samples having scores greater (or lesser) than the center point. In the context of our work, tasks represented six attributes and malignancy. We fine-tuned the network with these 7 tasks and performed 10 fold cross-validation. By fine-tuning the network, we circumvented the need to have a large amount of training data. Since the 3D network was trained on image sequences with 3 channels and with at least 16 frames, we replicated the same gray level axial channel for the other two.

Moreover, we also ensured that all input volumes have 16 slices by interpolation when necessary. We used the 4096-dimensional output from the first fully connected layer of the 3D CNN as a feature representation.

To find the structure matrix  $S$ , we computed the correlation between tasks by finding an initial normalized coefficient

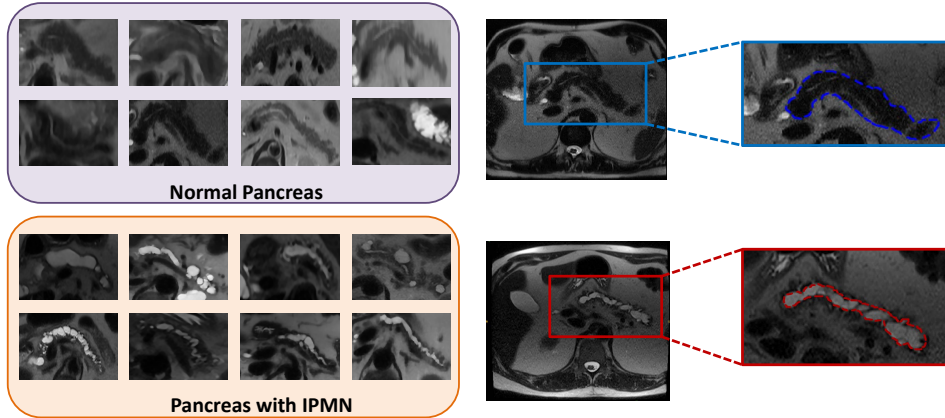


**Figure 4:** Axial T2 MRI scans illustrating pancreas. The top row shows different ROIs of pancreas, along with a magnified view of a normal pancreas (outlined in blue). The bottom row shows ROIs from subject with IPMN in the pancreas, which is outlined in red.

matrix  $\mathbf{W}$  using lasso with least square loss function and followed by computing the correlation coefficient matrix [24]. We then applied a threshold on the correlation coefficient matrix to obtain a binary graph structure matrix. The values for  $\rho_1$  and  $\rho_2$  were used as 1 and 10 respectively. For testing, we multiplied the features from network trained on malignancy with the corresponding coefficient vector  $W$  to obtain the score.

For evaluation, we used metrics for both classification and regression. We calculated classification accuracy by considering classification to be successful if the predicted score lies in  $\pm 1$  of the true score. We also reported average absolute score difference between the predicted score and the true score. Table I shows the comparison of our proposed MTL method with GIST features [28] +LASSO and 3D CNN MTL with trace norm. Our proposed graph regularized MTL outperforms the other methods with a significant margin. Our approach improves the classification accuracy over GIST features by about 15% and over trace norm regularization by 11%. Moreover, the average absolute score difference reduces by 32% and 27% when compared with GIST and trace norm respectively.

#### D. Evaluations and Results- Unsupervised Learning

For unsupervised learning, evaluations were performed on both lung nodules and IPMN datasets. In order to compute image level features, we used GIST descriptors [28]. The number of clusters is fixed as 2, which accounts for benign and malignant classes. The clustering result was checked to assign benign and malignant labels to the clusters. We used 10 fold cross-validation to evaluate our proposed approach. The training samples along with the label proportions generated using clustering served as the input to  $\infty$ SVM with a linear kernel.

For comparisons, we used accuracy, sensitivity and specificity as evaluation metrics. It can be observed in Table II that the proposed combination of clustering and  $\infty$ SVM significantly outperforms other approaches in accuracy and sensitivity. In comparison with clustering+SVM,

**TABLE II:** Average classification accuracy, sensitivity and specificity of the proposed *unsupervised* approach for IPMN and lung nodule classification with other methods

Evaluation Set	Methods	Accuracy	Sensitivity	Specificity
IPMN Classification	Clustering	49.18%	45.34%	<b>62.83%</b>
	Clustering + SVM	52.03%	51.96%	50.5%
	<b>Proposed approach</b>	<b>58.04%</b>	<b>58.61%</b>	41.67%
Lung Nodule Classification	Clustering	54.83%	48.69%	60.04%
	Clustering + SVM	76.04%	57.08%	<b>91.28%</b>
	<b>Proposed approach</b>	<b>78.06%</b>	<b>77.85%</b>	78.28%

the proposed framework yields almost 21% improvement in sensitivity for lung nodules and around 7% improvement for IPMN classification. The low sensitivity and high specificity of clustering and clustering+SVM approaches can be explained by disproportionate assignment of instances as benign (normal) by these two approaches, which is not found in the proposed approach. At the same time, the proposed approach records around 24% and 9% improvement in accuracy as compared to clustering for lung nodules and IPMN, respectively.

#### Are Deep Features good for Unsupervised Classification?

Given the success of deep learning features for image classification tasks and their popularity with the medical imaging community, we explored their performance to classify lung nodules and IPMN in an unsupervised manner. For this purpose, we used a pre-trained deep CNN architecture to extract features and then perform clustering to obtain baseline classification performance. We extracted features from fully-connected layers 7 and 8 of Fast-VGG [29] with and without applying ReLU non-linearity. Classification accuracy, using clustering over these features is shown in Figure 5.

It can be seen in Figure 5 that the features with non-linearity (ReLU) are more discriminative for classification using clustering as compared to without ReLU. The same trend can be observed for both lung nodules and IPMN classification using VGG-fc7 and VGG-fc8 layers. Owing

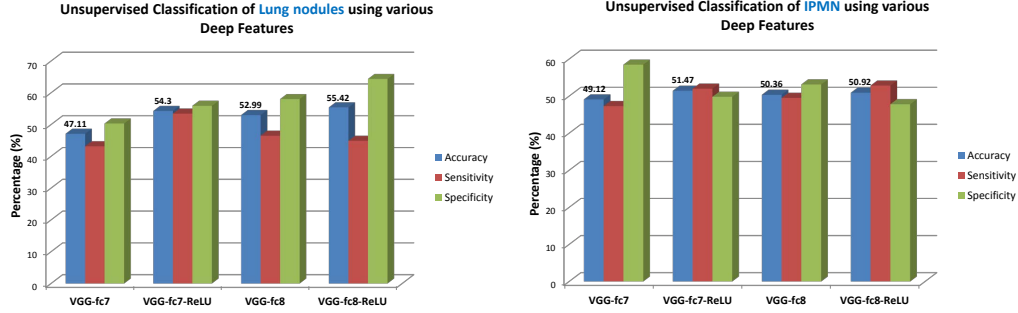


**Figure 5:** Influence of deep learning features obtained from different layers of a VGG network with and without ReLU non-linearities. The graph on the left shows accuracy, sensitivity and specificity for unsupervised lung nodule classification (clustering), whereas the right one shows the corresponding results for IPMN.

to the larger evaluation set, the influence of ReLU is more prominent for lung nodules as compared to IPMN. Although the results between VGG-fc7 and VGG-fc8 are not substantially different, highest accuracy for IPMN can be obtained by using VGG-fc7-ReLU features and for lung nodules by using VGG-fc8-ReLU features. The non-linearity induced by ReLU clips the negative values to zero, which can sparsify the feature vector and can reduce overfitting.

### Classification using Supervised Learning

In order to establish the upper-bound on the classification performance, we trained linear SVM and Random Forest using GIST and different deep learning features with ground truth labels on the same 10 fold cross-validations sets. Table III lists the classification accuracy, sensitivity, and specificity using GIST, VGG-fc7 and VGG-fc8 features for both IPMN and lung nodules. For both VGG-fc7 and VGG-fc8, we used features after ReLU since they are found to be more discriminative (Figure 5). Interestingly, for lung nodules, VGG-fc7 features along with RF classifier are reported to have comparable results to the combination of GIST and RF classifier. This can be explained by the fact that deep networks are pre-trained on ImageNet dataset as compared to handcrafted features such as GIST, which don’t require any training. On the other hand, for smaller datasets such as IPMN, deep features are found to perform better as compared to GIST. In order to balance the number of positive (IPMN) and negative (normal) examples, which can be a critical drawback otherwise, we performed Adaptive Synthetic Sampling [30]. This was done to generate synthetic examples in terms of features from the minority class (normal).

### Generative Adversarial Networks (GAN)

Recently, generative adversarial networks (GANs) [31] have gained considerable attention in deep learning and have been applied for different applications in visual domain [32], [33] including but not limited to image super-resolution, inpainting, video generation, etc.

GAN consists of a generator,  $\mathbf{G}$ , which aims to learn a distribution,  $p_z$  from noise, and a discriminator,  $\mathbf{D}$ , which sifts real data (sampled from true distribution  $p_{data}(x)$ ) from the artificial data (output of the generator). The two-player

minmax game between  $\mathbf{G}$  and  $\mathbf{D}$  is modeled with the following value function:

$$\min_{\mathbf{G}} \max_{\mathbf{D}} V(\mathbf{D}, \mathbf{G}) = \mathbb{E}_{x \sim p_{data}(x)} [\log(D(x))] + \mathbb{E}_{z \sim p_z(z)} [\log(1 - D(G(z)))], \quad (12)$$

where  $\mathbb{E}$  represents expectation.

In our work, we use Deep Convolutional GAN (DC-GAN) [32] to perform unsupervised representation learning and then use those representations to perform supervised classification. Our DC-GAN architecture is shown in Figure 6. The generator ( $\mathbf{G}$ ) comprises 3 deconvolution filters of sizes 128, 64 and 1 respectively. The discriminator consists of 2 convolutional layers of sizes 32 and 64 followed by a fully-connected layer of dimension 3136. We use features from FC layer of  $\mathbf{D}$  to train SVM and RF. Classification results using DC-GAN are shown in Table IV. The unsupervised feature representation with supervised classification reports comparable results to those obtained from the pre-trained network (Table III) for IPMN classification. For lung nodules, classification using pre-trained networks such as VGG outperforms classification over DC-GAN features.

## VI. DISCUSSION AND CONCLUDING REMARKS

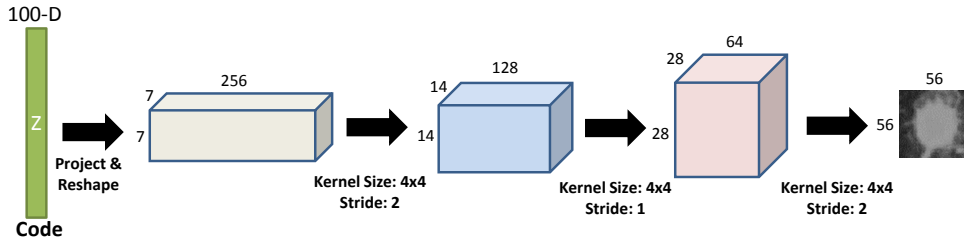
In this work, we proposed a framework to stratify the malignancy of lung nodules using 3D CNN and graph regularized sparse multi-task learning. To the best of our knowledge, this is for the first time, transfer learning is employed over 3D CNN to improve lung nodule characterization. The task of data collection, especially in medical imaging fields, is highly regulated and the availability of experts for annotating these images is restricted. In this scenario, leveraging on the availability of crowdsourced and annotated data such as user captured videos can be instrumental in training discriminative models. Given the diversity in data from these two domains (i.e. medical and non-medical user collected videos), it is vital to perform transfer learning from source domain (user collected videos) to the target domain (medical imaging data).

We also empirically explored the importance of high-level nodule attributes such as calcification, sphericity, lobulation, and others to improve malignancy determination. Rather than manually determining these attributes we used 3D CNN to



**TABLE III:** Classification of IPMN and Lung Nodules using different features and supervised learning classifiers.

Evaluation Set	Features	Classifiers	Accuracy (%)	Sensitivity (%)	Specificity (%)
IPMN Classification	GIST	SVM	76.05	83.65	<b>52.67</b>
		RF	81.9	93.69	43.0
	VGG-fc7	SVM	84.18	96.91	44.83
		RF	81.96	94.61	42.83
	VGG-fc8	SVM	<b>84.22</b>	<b>97.2</b>	46.5
		RF	80.82	93.4	45.67
Lung Nodule Classification	GIST	SVM	81.56	71.31	90.02
		RF	81.64	76.47	<b>85.97</b>
	VGG-fc7	SVM	77.97	75.2	80.6
		RF	<b>81.73</b>	<b>78.24</b>	84.59
	VGG-fc8	SVM	78.76	74.67	82.29
		RF	80.51	76.03	84.24

**Figure 6:** The generator architecture of DCGAN used to perform unsupervised representation learning.**TABLE IV:** Supervised classification for IPMN and Lung Nodules using unsupervised feature learning via Deep Convolutional Generative Adversarial Networks (DC-GAN)

Evaluation Set	Methods	Accuracy	Sensitivity	Specificity
IPMN Classification	SVM	<b>83.66</b>	<b>96.36</b>	42.83
	RF	81.37	93.92	<b>44.50</b>
Lung Nodule Classification	SVM	75.09	68.31	80.41
	RF	<b>77.96</b>	<b>72.53</b>	<b>82.45</b>

learn discriminative features corresponding to these attributes. The 3D CNN based features from these attributes are fused in a graph regularized sparse MTL.

In the second part of this study, we explored the potential of unsupervised learning for malignancy determination. Since in most medical imaging tasks radiologists are required to get annotations, acquiring labels to learn machine learning models is more cumbersome and expensive as compared to other computer vision tasks. In order to address this challenge, we employed clustering to obtain an initial set of labels. Since the instance level labels obtained from clustering may not be reliable enough to train a discriminative classifier, we used label proportions obtained from clustering to train a  $\alpha$ SVM. Our proposed combination of clustering and  $\alpha$ SVM outperformed the other methods in evaluation metrics.

Following up on the application of deep learning for almost all tasks in the visual domain, we studied the influence of different pre-trained deep networks for lung nodule classification. For some instances, we found that commonly used imaging features such as GIST have comparable results as those obtained from pre-trained network features. This observation can be explained by the fact that the deep networks were trained on ImageNet classification tasks so the filters in CNN were more

tuned to the nuances in natural images as compared to medical images. In order to set a performance upper bound, we also evaluated supervised learning using different combinations of features and classifiers. We also explored the application of unsupervised feature representation using DC-GAN for IPMN and lung nodule classification tasks.

To the best of our knowledge, this is one of the first and the largest evaluation of a CAD system for IPMN classification. CAD systems for IPMN classification are relatively newer research problems and there is a need to explore the use of different imaging modalities to improve classification. Although MRI remains the most common modality to study pancreatic cysts, CT images can also be used as a complementary imaging modality due to its higher resolution and its ability to capture smaller cysts. Additionally, a combination of T2-weighted, contrast-enhanced and unenhanced T1-weighted sequences can help improve detection and diagnosis of IPMN [19]. In this regard, multi-modal deep learning architectures can be deemed useful [34]. Additionally, in this work, we used a manually detected ROI for IPMN classification. Our future work will involve joint localization (detection) and classification of IPMN.

The future prospects of using different architectures to improve GAN training are promising. Instead of using hand-engineered priors of sampling in the generator, the work in [35] learned priors using denoising auto-encoders. In order to measure sample similarity for complex distributions such as those in the images, [36] jointly trained variational auto-encoders and GANs. Moreover, the applications of CatGAN [37] and InfoGAN [38] for semi-supervised and unsupervised classification tasks in medical imaging are worth exploring as well.

Incorporating unsupervised learning within the deep learning framework for malignancy determination will be another dimension to explore. For lung nodules, another important

imaging modality is Positron Emission Tomography (PET). It has been found that the combination of PET and CT can improve the diagnostic accuracy of solitary lung nodules [39]. With the increase in the availability of PET/CT scanners, our future work will involve their utilization for simultaneous detection and characterization of pulmonary nodules.

## REFERENCES

- [1] Society, A.C.: Cancer Facts & Figures. American Cancer Society (2016)
- [2] Sadot, E., Basturk, O., Klimstra, D.S., Gönen, M., Anna, L., Do, R.K.G., D'Angelica, M.I., DeMatteo, R.P., Kingham, T.P., Jarnagin, W.R., et al.: Tumor-associated neutrophils and malignant progression in intraductal papillary mucinous neoplasms: an opportunity for identification of high-risk disease. *Annals of surgery* 262(6), 1102 (2015)
- [3] Kumar, D., Wong, A., Clausi, D.A.: Lung nodule classification using deep features in CT images. In: *Computer and Robot Vision (CRV)*, 2015 12th Conference on. pp. 133–138. IEEE (2015)
- [4] Buty, M., Xu, Z., Gao, M., Bagci, U., Wu, A., Mollura, D.J.: Characterization of Lung Nodule Malignancy Using Hybrid Shape and Appearance Features. In: *International Conference on Medical Image Computing and Computer-Assisted Intervention (MICCAI)*. pp. 662–670. Springer (2016)
- [5] Hussein, S., Cao, K., Song, Q., Bagci, U.: Risk Stratification of Lung Nodules Using 3D CNN-Based Multi-task Learning. In: *International Conference on Information Processing in Medical Imaging*. pp. 249–260. Springer (2017)
- [6] Shin, H., Roth, H.R., Gao, M., Lu, L., Xu, Z., Nogues, I., Yao, J., Mollura, D., Summers, R.M.: Deep convolutional neural networks for computer-aided detection: CNN architectures, dataset characteristics and transfer learning. *IEEE Transactions on Medical Imaging* 35(5), 1285–1298 (2016)
- [7] Tran, D., Bourdev, L., Fergus, R., Torresani, L., Paluri, M.: Learning spatiotemporal features with 3D convolutional networks. In: *2015 IEEE International Conference on Computer Vision (ICCV)*. pp. 4489–4497. IEEE (2015)
- [8] Furuya, K., Murayama, S., Soeda, H., Murakami, J., Ichinose, Y., Yauuchi, H., Katsuda, Y., Koga, M., Masuda, K.: New classification of small pulmonary nodules by margin characteristics on high-resolution CT. *Acta Radiologica* 40(5), 496–504 (1999)
- [9] Uchiyama, Y., Katsuragawa, S., Abe, H., Shiraishi, J., Li, F., Li, Q., Zhang, C.T., Suzuki, K., Doi, K.: Quantitative computerized analysis of diffuse lung disease in high-resolution computed tomography. *Medical Physics* 30(9), 2440–2454 (2003)
- [10] El-Baz, A., Nitzken, M., Khalifa, F., Elnakib, A., Gimelfarb, G., Falk, R., El-Ghar, M.A.: 3D shape analysis for early diagnosis of malignant lung nodules. In: *Biennial International Conference on Information Processing in Medical Imaging*. pp. 772–783. Springer (2011)
- [11] Han, F., Wang, H., Zhang, G., Han, H., Song, B., Li, L., Moore, W., Lu, H., Zhao, H., Liang, Z.: Texture feature analysis for computer-aided diagnosis on pulmonary nodules. *Journal of Digital Imaging* 28(1), 99–115 (2015)
- [12] Way, T.W., Hadjiiski, L.M., Sahiner, B., Chan, H.P., Cascade, P.N., Kazerooni, E.A., Bogot, N., Zhou, C.: Computer-aided diagnosis of pulmonary nodules on CT scans: segmentation and classification using 3D active contours. *Medical Physics* 33(7), 2323–2337 (2006)
- [13] Lee, M., Boroczky, L., Sungur-Stasik, K., Cann, A., Borczuk, A., Kawut, S., Powell, C.: Computer-aided diagnosis of pulmonary nodules using a two-step approach for feature selection and classifier ensemble construction. *Artificial Intelligence in Medicine* 50(1), 43–53 (2010)
- [14] Chen, S., Ni, D., Qin, J., Lei, B., Wang, T., Cheng, J.Z.: Bridging computational features toward multiple semantic features with multi-task regression: A study of CT pulmonary nodules. In: *International Conference on Medical Image Computing and Computer-Assisted Intervention*. pp. 53–60. Springer (2016)
- [15] Zhou, Y., Xie, L., Fishman, E.K., Yuille, A.L.: Deep Supervision for Pancreatic Cyst Segmentation in Abdominal CT Scans. *arXiv preprint arXiv:1706.07346* (2017)
- [16] Cai, J., Lu, L., Zhang, Z., Xing, F., Yang, L., Yin, Q.: Pancreas segmentation in MRI using graph-based decision fusion on convolutional neural networks. In: *International Conference on Medical Image Computing and Computer-Assisted Intervention*. pp. 442–450. Springer (2016)
- [17] Hanania, A.N., Bantis, L.E., Feng, Z., Wang, H., Tamm, E.P., Katz, M.H., Maitra, A., Koay, E.J.: Quantitative imaging to evaluate malignant potential of IPMNs. *Oncotarget* 7(52), 85776 (2016)
- [18] Gazit, L., Chakraborty, J., Attiye, M., Langdon-Embry, L., Allen, P.J., Do, R.K., Simpson, A.L.: Quantification of CT Images for the Classification of High-and Low-Risk Pancreatic Cysts. In: *SPIE Medical Imaging*. pp. 101340X–101340X. International Society for Optics and Photonics (2017)
- [19] Kalb, B., Sarmiento, J.M., Kooby, D.A., Adsay, N.V., Martin, D.R.: MR imaging of cystic lesions of the pancreas. *Radiographics* 29(6), 1749–1765 (2009)
- [20] Sivic, J., Russell, B.C., Efros, A.A., Zisserman, A., Freeman, W.T.: Discovering objects and their location in images. In: *Computer Vision, 2005. ICCV 2005. Tenth IEEE International Conference on*. vol. 1, pp. 370–377. IEEE (2005)
- [21] Kamper, H., Jansen, A., Goldwater, S.: Fully unsupervised small-vocabulary speech recognition using a segmental Bayesian model. In: *Interspeech* (2015)
- [22] Armato III, S., McLennan, G., Bidaut, L., McNitt-Gray, M.F., Meyer, C.R., Reeves, A.P., Zhao, B., Aberle, D.R., Henschke, C.I., Hoffman, E.A., et al.: The Lung Image Database Consortium (LIDC) and Image Database Resource Initiative (IDRI): a completed reference database of lung nodules on CT scans. *Medical Physics* 38(2), 915–931 (2011)
- [23] Karpathy, A., Toderici, G., Shetty, S., Leung, T., Sukthankar, R., Fei-Fei, L.: Large-scale video classification with convolutional neural networks. In: *Proceedings of the IEEE conference on Computer Vision and Pattern Recognition*. pp. 1725–1732 (2014)
- [24] Zhou, J., Chen, J., Ye, J.: MALSAR: Multi-task learning via structural regularization (2012)
- [25] Nesterov, Y.: *Introductory lectures on convex optimization: A basic course*, vol. 87. Springer Science & Business Media (2013)
- [26] Yu, F., Liu, D., Kumar, S., Tony, J., Chang, S.F.:  $\alpha$ SVM for Learning with Label Proportions. In: *Proceedings of The 30th International Conference on Machine Learning*. pp. 504–512 (2013)
- [27] Tustison, N.J., Avants, B.B., Cook, P.A., Zheng, Y., Egan, A., Yushkevich, P.A., Gee, J.C.: N4ITK: Improved N3 bias correction. *IEEE Transactions on Medical Imaging* 29(6), 1310–1320 (2010)
- [28] Oliva, A., Torralba, A.: Modeling the shape of the scene: A holistic representation of the spatial envelope. *International Journal of Computer Vision* 42(3), 145–175 (2001)
- [29] Chatfield, K., Simonyan, K., Vedaldi, A., Zisserman, A.: Return of the devil in the details: Delving deep into convolutional nets. In: *British Machine Vision Conference* (2014)
- [30] He, H., Bai, Y., Garcia, E.A., Li, S.: ADASYN: Adaptive synthetic sampling approach for imbalanced learning. In: *Neural Networks, 2008. IJCNN 2008. (IEEE World Congress on Computational Intelligence)*. IEEE International Joint Conference on. pp. 1322–1328. IEEE (2008)
- [31] Goodfellow, I., Pouget-Abadie, J., Mirza, M., Xu, B., Warde-Farley, D., Ozair, S., Courville, A., Bengio, Y.: Generative Adversarial Nets. In: *Advances in Neural Information Processing Systems*. pp. 2672–2680 (2014)
- [32] Radford, A., Metz, L., Chintala, S.: Unsupervised representation learning with deep convolutional generative adversarial networks. *arXiv preprint arXiv:1511.06434* (2015)
- [33] Schlegl, T., Seeböck, P., Waldstein, S.M., Schmidt-Erfurth, U., Langs, G.: Unsupervised Anomaly Detection with Generative Adversarial Networks to Guide Marker Discovery. In: *International Conference on Information Processing in Medical Imaging*. pp. 146–157. Springer (2017)
- [34] Ma, L., Lu, Z., Shang, L., Li, H.: Multimodal convolutional neural networks for matching image and sentence. In: *Proceedings of the IEEE International Conference on Computer Vision*. pp. 2623–2631 (2015)
- [35] Nguyen, A., Yosinski, J., Bengio, Y., Dosovitskiy, A., Clune, J.: Plug & play generative networks: Conditional iterative generation of images in latent space. *arXiv preprint arXiv:1612.00005* (2016)
- [36] Larsen, A.B.L., Sønderby, S.K., Larochelle, H., Winther, O.: Autoencoding beyond pixels using a learned similarity metric. In: *33rd International Conference on Machine Learning (ICML 2016) International Conference on Machine Learning* (2016)
- [37] Springenberg, J.T.: Unsupervised and semi-supervised learning with categorical generative adversarial networks. *arXiv preprint arXiv:1511.06390* (2015)
- [38] Chen, X., Duan, Y., Houthoofd, R., Schulman, J., Sutskever, I., Abbeel, P.: Infogan: Interpretable representation learning by information maximizing generative adversarial nets. In: *Advances in Neural Information Processing Systems*. pp. 2172–2180 (2016)
- [39] Wang, Y.X.J., Gong, J.S., Suzuki, K., Morcos, S.K.: Evidence based imaging strategies for solitary pulmonary nodule. *Journal of thoracic disease* 6(7), 872–887 (2014)